Journal of Civil Engineering Researchers

J-Researchers

JOURNAL OF CIVIL ENGINEERING RESEARCHERS

Comprehensive Investigation of the Omega-Shaped Hybrid CFRP Sheet - Concrete Slab System: Experimental, Numerical and Analytical study

Amir Mohammad Bakhtiari,[a,*] Ali Harati[a]

[a] *Department of Civil Engineering, Arman Institution of Engineering and Technology, Tehran, Iran*

Journals-Researchers use only: Received date: 2023.06.21; revised date: 2023.08.05; accepted date: 2023.09.23

Abstract

Fiber Reinforced Polymer (FRP) composites have been broadly applied in substitution of steel members at rehabilitation interventions thanks to their lightweight, high strength, and high corrosion resistance. Producing novel FRP-concrete hybrid structures is the next step researchers are dealing with. In this context, the present study focuses on the numerical and analytical modeling of the experimentally obtained response of hybrid FRP-concrete slabs subjected to three points bending tests. The analyzed hybrid elements consisted of an omega shape Carbon Reinforced Polymer (CFRP) sheet on which a concrete layer was cast forming a unidirectional slab member. A Glass Fiber Reinforced Polymer (GFRP) fabric was bonded to the CFRP sheet and embedded into the concrete block to provide a connection between CFRP and concrete in one of the specimens. Simulation results showed agreement with the experimental response in terms of load-displacement curve, concrete plastic strain and failure mode. After validating the model, alternative designs (width, height, and thickness of CFRP sheet and concrete block on it) were numerically tested to study the influence of the geometry of the structural system on the load-bearing capacity. Lastly, analytical formulation assuming total compatibility and based on Euler-Bernoulli theory were implemented and contrasted with the experimental response. Overall results pointed out that the optimum design would be the one with increased height of both concrete and CFRP. For this improved configuration, the load-bearing capacity was increased by up to 44%. (DOI:**https//doi.org/10.52547/JCER.5.4.41**)

Keywords: Hybrid FRP-concrete; Carbon Fiber Reinforced Polymer (CFRP); Numerical model; Flexural behavior; Analytical model

1. Introduction

In bridges and high-rise buildings, steel-concrete composite structures are frequently used, especially composite floor systems consisting of a concrete deck poured on top of corrugated steel sheets [1], [2]. Considerations such as profile design, steel sheet width, concrete compressive strength, span, shear connectors and steel-concrete interface shear bond

* Corresponding author. Tel.: +989125148269; e-mail: bakhtiariamir96@gmail.com.

also affect the strength and performance of steel-concrete composite slabs [3], [4]. Over the last decades, extensive experiments have been carried out on the structural efficiency of one and two-span composite slabs with concrete and steel sheeting with or without embossing or mechanical connectors. In addition, researchers have performed a wide variety of finite element simulations of these composite slabs [5], [6]. Full scale tests of composite slabs were accurately modelled in the research by Veljkovic [7]. Numerical model results were compared with available experimental data of two types composite slabs and the corresponding m-k characterization by Eurocode-4. The outcomes confirmed the validity of the model and its simplicity with respect to other available models since a reduced number of variables were required to predict the structural behavior of the slabs in [8]. A general FEM (Finite Element Model) approach of composite sections was introduced in [9], in which the shear bond cooperation between the steel deck and the concrete was treated as a contact issue characterized by cohesion and friction. Comparison between experimental and FEM outcomes showed that the FEM analysis depended on the interface contact model. Model was capable of accurately predicting the performance and the load carrying capacity of composite slabs. Another procedure to implement 3D non-linear FEM models was introduced to simulate the longitudinal slip mechanics of composite slabs in "pull-out" tests [10].

It was also found, though, that these kinds of systems have problems with corrosion. It is well-known that the strength and stiffness of reinforced concrete and steel structures can be lost due to corrosion [11], Arc-spot welds (puddle welds) or screw pins (Hilti-screws) are currently used during construction to briefly fasten the metal deck sheets on top of the supporting members, promoting additional corrosion issues [12].

Because of durability it has been proposed to replace steel members by fiber composite ones. This substitution may allow easier and quicker building procedures that led to the workers' welfare and economic savings [13], [14]. These benefits would enable residential buildings to use the composite floor structure and make it more effective in manufacturing applications [15], [16]. Several pioneers have experimented with hybrid fiber-reinforced polymer (FRP)-concrete systems to address steel disadvantages [17].

However, the initial researches on FRP applications in building industry used fiber-reinforced polymer (FRP) profiles and laminates to strengthen concrete and masonry structures. FRP has become one of the key technologies for restoring and retrofitting existing structures as a result of the last decade's investigations. Deficiencies such as reinforcement erosion, concrete decay, and damage resulting from aging are commonly observed in Reinforced Concrete (RC) structures constructed in the last century [18], [19]. In this context, FRP strengthening elements were originally used in RC systems, resulting in greater corrosion resistance [20]. Smaller work crews, smaller machinery, and smaller supporting structures during construction are also needed for the FRP strengthening or hybrid FRP-concrete structures [21]. All these benefits resulted in improved FRP structures, such as applications with low stress, that perform better, last long, cost-effectively and with lower long-term maintenance costs in comparison to steel ones [22]. Since the mid-1990s, FRP deck implementations have gradually been introduced in the United States. Comprehensive research on stiffness and strength tests of different types of FRP decks with concrete top layer were undertaken [23].

On this basis, it is suggested the latest research on hybrid FRP profile-concrete structures and the existing composite steel sheet-concrete slabs to be combined to introduce new hybrid FRP sheet-concrete slabs. Modelling this novel type of structures is a must to discuss about their structural performance and to compare with the little existing experimental evidences. Two specimens were produced, tested and simulated to calibrated the numerical model aimed to accurately represent the experimentally obtained loading branch of two of these novel hybrid FRP-sheet – concrete slabs. Once validated, the numerical model was used for designing theoretical cases and it was applied to assess the specimens' optimum geometric configuration. This particular secondary numerical study included changes in height of concrete and CFRP, length and width of hybrid slab, and also changes in CFRP's dimensions, resulting in five additional theoretical cases.

On the overall, this research attempts to provide design guidelines for hybrid FRP-concrete slab

elements which can achieve the great benefits of FRP and hybrid steel-concrete slabs but overcoming steel sheet disadvantages.

Finally, an analytical calculation proposal on the basis of Euler-Bernoulli hypothesis is also investigated for simplicity and comparison with numerical model results

2. Experimental tests

Two carbon fiber reinforced polymer (CFRP) omega shape sheet – concrete hybrid slabs were tested. One of them had an only chemical connection on the CFRP-concrete interface by direct adhesion with no additional products. The other specimen included aggregate particles bonded to the inner face of the CFRP sheet. These particles were considered to increase frictional response and improve pre-sliding connection. Besides, this second specimen had a glass fiber fabric bonded to the top surfaces of the CFRP omega shape to improve the CFRP-concrete connection. Material properties, specimens' dimensions, experimental setup, and results of these tests used to fit the model are summarized herein.

2.1. Materials and specimens

Specimens' dimensions, CFRP and mesh configurations are shown in Figure 1. The average concrete properties were 21 MPa, 2.75 MPa, and 24 GPa for compressive strength, tensile strength, and modulus of elasticity respectively. These were obtained according to CEB-FIB [24]. Epoxy resin was used for laminating CFRP sheets, the properties of the resin were experimentally obtained with 8000 MPa, 95.5 MPa, and 23.0 MPa, respectively, for modulus of elasticity, compressive and tensile strength [25]. The average values of elastic modulus and ultimate tensile strength of CFRP sheets were 45550 MPa and 1120 MPa, respectively based on standard [26]. The thickness of the CFRP sheet was 2mm. Glass fiber mesh (alkali-resistant fiberglass) were applied as CFRP-concrete connectors. Mesh was bonded to the top surface of omega-shape CFRP using the same epoxy resin previously used for CFRP production. These meshes were used with dimensions of 2000mm × 400mm. Mechanical properties were ultimate tensile strength of 45kN/m and ultimate elongation of 0.018.

The same epoxy resin was used for laminating CFRP, bonding aggregates, and bonding glass fiber mesh. After casting CFRP laminates with the help of steel omega shape frame and edges' wooden frames, installing mesh on the crests with resin (in with mesh specimen) and concreting have been performed. Figure 1.b. shows specimen (with mesh) before concreting.

2.2. test setup

Three-point bending tests were conducted on simply supported specimens. The free span was 1800mm (L) and the load (F) was indirectly applied through an imposed downward displacement (Δ) at a rate of 1 mm/min until specimen failure. An oleo-hydraulic actuator of 50kN force range and 150mm displacement range equipped with a load cell and an LDVT was used for this purpose. A steel profile HEB120 was used as a loading tool for load distribution along slab width. Vertical displacement was also measured externally with two 100 mm range potentiometers with a linearity of 0.2 percent at the load application section. Two external LVDTs with a range of 20 mm and linearity of 0.2 percent were used to measure the relative longitudinal displacement between the CFRP sheet and the concrete block at both ends. Finally, at mid-span position on the external face of the CFRP sheet, two strain gauges of 350 ohms resistance connected with 4 wires were installed, Figure 2shows boundary and loading conditions of the experimental test setup.

2.3. Results of bending tests

The results of the experimented Omega Shape slabs in terms of load, deflection, relative yield displacement (dy), maximum relative displacement (du), general ductility ratio (μ) of the slab, dissipated energy and deformation at the maximum capacity and modes of failure, are reported in Table 1. The Force-displacement curve response for both considered experimental cases is shown in Figure 3.

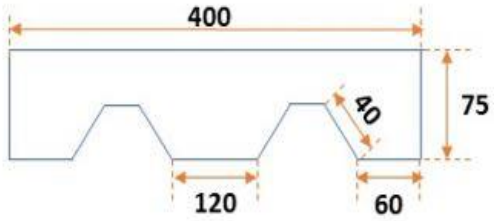

a. Concrete section

b. specimen (with mesh) before concreting

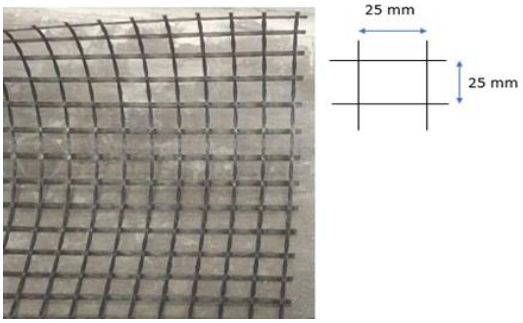

c. Glass fiber mesh

d. Carbon fiber

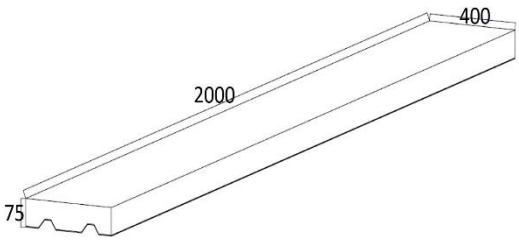

e. Whole model dimensions

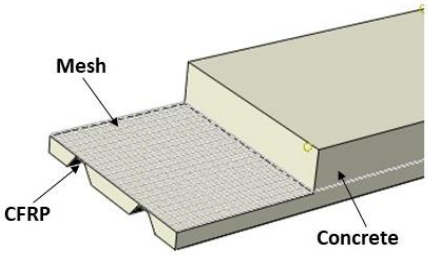

f. Schematic of main components

Figure 1. Experimental details and dimensions

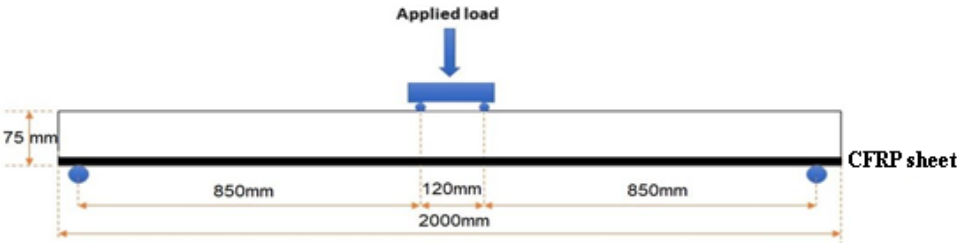

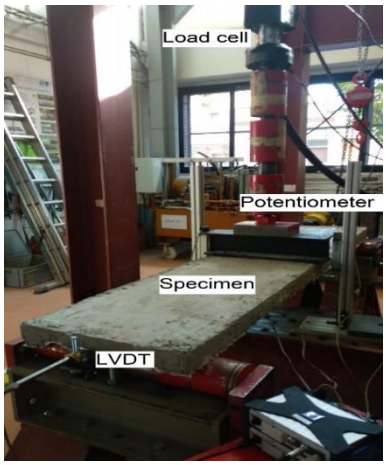

Figure 2. Boundary and loading conditions of the experimental test setup

Table 1.
Experimental results

Specimen	Maximum strength (kN)	Fu	Deformation at the maximum capacity (mm)	dy (mm)	du (mm)	dissipated energy (kN.mm)	$\mu = \frac{d_u}{d_y}$	Failure mode
With mesh	20.61	14.94	29.44	18.03	29.44	344.18	1.63	CFRP-concrete debonding
Without mesh	11.55	8.32	24.34	13.24	24.34	168.71	1.83	CFRP-concrete debonding

These are divided into two main parts; the first part corresponded with a linear-elastic response with a constant slope which ended with the first crack development and the second one showed a nonlinear slope in both specimens, also including the post cracking stage. Figure 4-a and Figure 4-b depict the failure mode of the experimented Concrete Omega Shape slab with and without mesh respectively. Both specimens failed by CFRP-concrete debonding, although the one with no mesh reached lower load-bearing capacity as shown in Figures 4-a and 4-b.

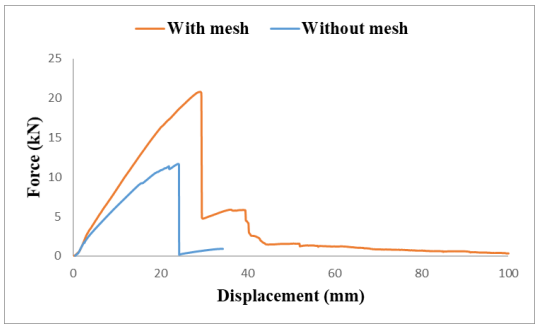

Figure 3. Force-Displacement curves obtained by experimental results

3. Finite element method (FEM)

ABAQUS [27] general-purpose finite element software was used to model experimental tests to provide a general procedure widely available for practitioners. Geometry, materials, mesh, boundary conditions, contacts, and calculation procedure definitions of the implemented model are described.

Geometry was defined according with definition of specimens (section 2.1). Concrete was represented by a single 3D part, CFRP omega-shape sheet was represented as 2D plate and the mesh was represented by 1D truss elements according to its geometric definition.

Concrete Damage Plasticity (CDP) was used in the composite slab simulation to define concrete behavior in FE modeling. The CDP model was developed based

on two concrete failure mechanisms: compressive crushing and tensile cracking [28], [29]. It combines isotropic damaged elasticity with isotropic tensile and compressive plasticity. Tensile cracking and compressive crushing of concrete are considered the two main failure mechanisms [30]. The following values for the Poisson's ratio (0.15) and dilation angle Ψ (30^0) were selected according to the literature [31–34] For nonlinear uniaxial behavior of concrete, the Kent and Park formulation was used [35]. According to this, compressive stress is calculated by equation (1):

$$\sigma_C = f'_{co}\left[2\left(\frac{\varepsilon_c}{\varepsilon'_c}\right) - \left(\frac{\varepsilon_c}{\varepsilon'_c}\right)^2\right] \quad (1)$$

(a)With mesh

(b)Without the mesh

Figure 4. Cracking pattern on the tension surface.

Where $\varepsilon_c$is a compressive strain, f'_{co} and ε'_c are the compressive strength of unconfined cylindrical concrete specimen and the related strain respectively. The value of ε'_c is considered to be 0.002.

The compression damage parameter (d_c), controls the unloading gradient of the stress-strain curve. In concrete and similar materials, such as masonry materials, the higher the plastic strain, the slope of the unloading curve will be reduced to a greater extent than the initial gradient (elasticity specimen). It is due to the damage caused by the loss induced in a brittle material. When damage starts, compressive stress is calculated based on the following equations (2) and (3) [36–38]:

$$\sigma_C = (1 - d_c)\, E_O\, (\varepsilon_C - \varepsilon_C{}^{\sim PL}) \quad (2)$$

$$\varepsilon_C{}^{\sim PL} = \left(\varepsilon_C{}^{\sim in} - \frac{1}{(1 - d_{c)}}\frac{\sigma_c}{E_0}\right) \quad (3)$$

Where $\varepsilon_C{}^{\sim PL}$ is an inelastic strain, ε_C is the compressive strain, E_O is elasticity modulus, d_c is compressive damage, $\varepsilon_C{}^{\sim in}$ is strain related to damage.

Finally, equation 4 is used to calculate the compressive damage value d_c [39]:

$$dc = 1 - \frac{\sigma_c}{f'_{co}} \quad (4)$$

Finally, to completely define the CDP material yield surface, dilation angle (Ψ), the ratio of the second stress invariant on the tensile meridian (K_c) and the viscosity parameter (μ) were defined. Ψ = 30, K_c = 0.667 and μ = 0.001 were recommended values by Abaqus [40]. Higher values of the dilation angle yield ductile response while lower values yield fragile response. Calculated damage parameter in compression (d_c) has remarkable influence on the bending response of concrete elements. Using greater viscosity parameter can considerably decrease the computational time, but results fitting is expected to be poorer. Thus, the choice of the viscosity parameter value in practicable calculations using the CDP material model should be constructed with great care and calibrated accordingly.

The concrete stress–strain compression relationship and the tensile post cracking behavior of concrete was defined according to CEB-FIB [24].

Two node linear 3-D truss elements (T3D2) were used to simulate the internal glass fiber mesh, 3D-solid elements (C3D8R) were used to discretize concrete volume and 3-node triangular general-purpose shell elements (S3R) were used for CFRP slab. Different mesh sizes depending on the thickness of each part (concrete, glass fiber mesh, and CFRP sheet) were used. The convergence of the numerical solutions was checked by using mesh sizes of 100, 75, 50, and 25 mm in the mesh and CFRP shell, resulting in selecting a 50mm mesh and CFRP shell size.

The contact between CFRP and concrete was assumed to be perfectly bonded (tie). Interaction

between glass fiber mesh and concrete was modeled as an embedded region and interactions between glass fiber mesh and CFRP were also are a tie. The slab model was simply supported at the corresponding span and the load was indirectly modeled as an imposed displacement of an area of 400mm x 120mm that was located on the top face in the middle of the slab. The reaction force associated with this imposed displacement was taken as the applied force. The procedure of analysis was done in implicit mode. Regarding quasi-static loading, the static general step was selected for analysis. For running seven models, calculation time was approximately 17 hours with Intel® core i7 CPU.

4. Model fitting

For the best fitting, the values corresponding to dilation angle, Kc, and viscosity parameter were taken as equal to 30, 1.16, and 0.667, respectively. These values met Abaqus recommendations for Concrete Damaged Plasticity and other researcher's data [41].

The results for the best fitting parameters are reported in Table 2 and shown in Figure 5. Good agreement can be seen between the experimental and numerical curves. In particular, maximum loads were predicted with an average relative error of 4.7% (19.58kN predicted vs. 20.61kN experimental for the cases with mesh and 11.05kN vs. 11.55kN for the cases without mesh). The numerical model tends to slightly underestimate experimental load-bearing capacity.

Regarding the stiffness, the model accurately predicts the force-displacement slope. Secant stiffness defined between 20% and 80% of the maximum load had an average relative error of 4.3% respect experimental results. Thus, the implemented model accurately predicts the loading branch as originally aimed. As long as the CFRP-concrete contact was supposed to be completely bonded, when this condition is lost the model convergence is no longer possible and there is no predicted data for the poet-critic response. Thus, FEM failure mode was CFRP-concrete disconnection, indicating that experimental failure mode was also correctly predicted.

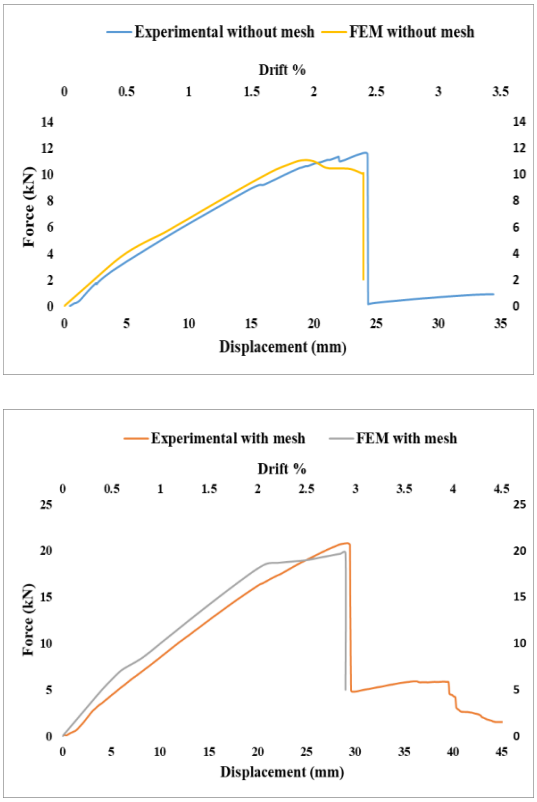

Figure 5. The experimental and numerical load-deflection curves of the specimen slab with and without mesh

5. Geometric parameters study

To evaluate the performance of the full hybrid omega shape CFRP sheet-concrete slab various geometries were simulated with the parameters fixed in the previous fitting process. The cases simulated with the previously validated model are summarized in Table 2 and Figure 6.

In Figure 7, force-displacement curves of cases A, B, C, D, and E are represented together with that representing experimental tested cases. Curve of case D was modified so to be comparable to the same width of the rest of the cases by multiplying force by the factor 400/480. In Table 2, the values of ultimate strength (F_p), Deformation at the maximum capacity (d_u), and the area beneath the force-displacement curve (dissipated energy-G_d) are introduced.

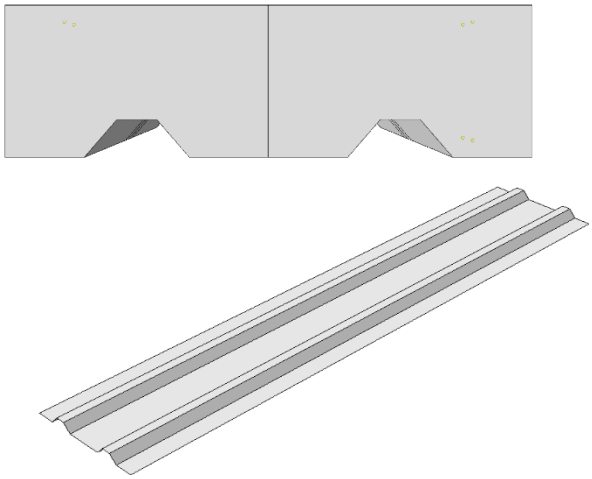

1) Case A. Increased concrete height

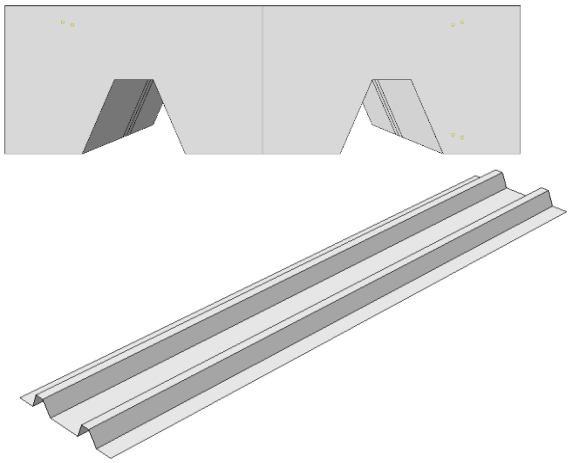

2) Case B. Increased concrete and CFRP height

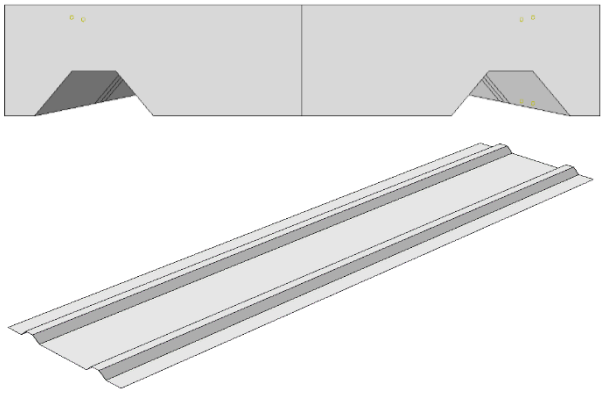

3) Case C. Increased distance between crests

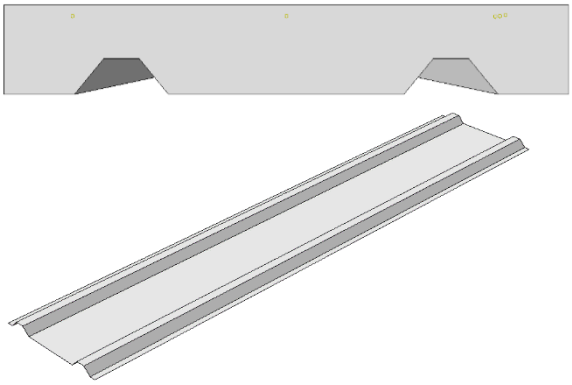

4) Case D. Increased concrete width and distance between crests

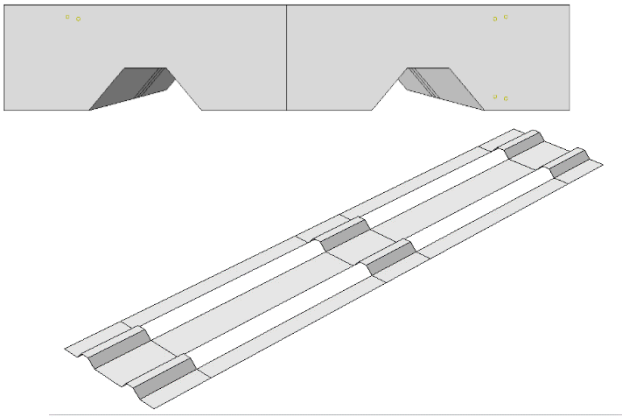

5)

Figure 6. Definition of hybrid omega shape CFRP sheet – concrete specimens for geometry parametric study.

Table 2.
Theoretical simulations

Case	Mesh	Concrete height (mm)	Concrete width (mm)	CFRP omega height (mm)	CFRP omega distance (mm)	CFRP continuity
With mesh	Yes	75	400	35	120	Continuous
Without mesh	No	75	400	35	120	Discontinuous
Case A	Yes	120	400	35	120	Continuous
Case B	Yes	120	400	60	120	Continuous
Case C	Yes	75	400	35	200	Continuous
Case D	Yes	75	480	35	200	Continuous
Case E	Yes	75	400	35	120	Discontinuous

Results showed that increasing the concrete cross-section significantly increased the load-bearing capacity. Cases A and B showed similar capacities, so increasing the height of the CFRP is no effect if the CFRP-concrete connection is assured. Case A had a greater concrete area so showed greater initial stiffness although the larger CFRP area of the B case brought higher maximum resistance. In the case of C, increasing the distance between Omega shapes reduces the CFRP amount in the center of the slab causing a reduction in the system's dissipated energy in comparison with the case With Mesh, although the maximum load-bearing capacity was maintained. Comparing case D with cases A and B showed that increasing the cross-section height is more effective than increasing the cross-section width against bending as it was expected. A comparison of case E with the experimental case with mesh revealed that reducing CFRP caused a decrease in the load-bearing capacity.

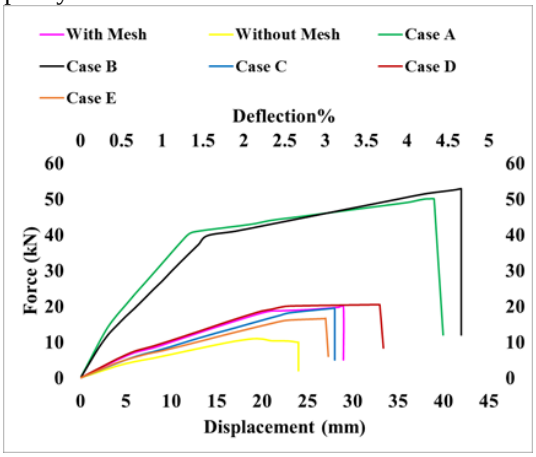

Deflection = (Δ*100)/(L/2) Δ: Vertical displacement in mid-span L: Length of the slab

Figure 7. Comparison of Force-Displacement curves for cases.

5.1. Analysis of the maximum plastic strain index

The ultimate plastic strain (PE) criterion is an appropriate parameter in estimating the damage in concrete. This is a suitable criterion for investigating the number of cracks and the tensile and compression failures along with their alignment. Concrete damage is related to the CFRP-concrete debonding process. However, enhancing capability depends on the integrity of the CFRP-concrete interface. The end of the CFRP plates is vulnerable to stress concentration, which can contribute to the emergence of micro-cracks at an early stage. Debonding failure happens initially at very small cracks and then expands to other parts of the structure. Debonding cracks in the internal interface of the framework are difficult to find in the engineering field. When cracks are linked to each other, the ability of the system would instantly collapse, which could ultimately lead to a huge loss of life and property [42]. Although these particular parameters are useful for evaluating the amount of damaged concrete, PE is more commonly used [41].

The model for the experimental case with mesh reached a maximum plastic strain value of about 1.23%, which indicated extensive tensile damage in concrete, and most of the cracks were formed at the center of the slab. Greatest cracks in this area were expected and obtained by the model as can be seen in Figure 8 and Table 3. If removing the mesh, the maximum principal plastic strain is increased to about 1.70% indicating a stress concentration and the corresponding damage increase.

Increasing the concrete height (case A) can significantly improve the bending capacity of the system and transfer the cracks out of the center of the slab region.

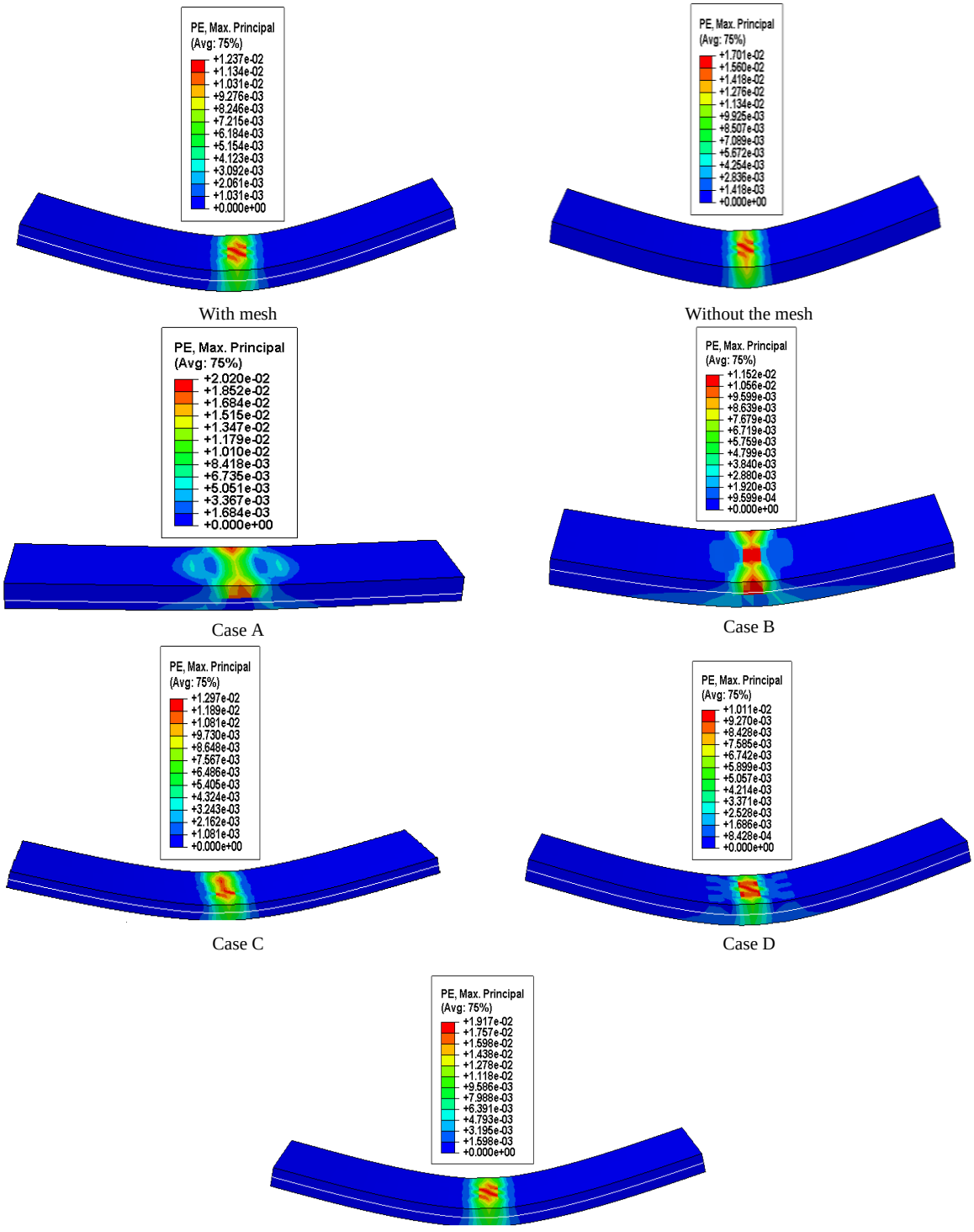

Figure 8. Maximum principal plastic strain in the base and the proposed cases

Table 3.
The maximum load-carrying capacity, the dissipated energy, and maximum principle plastic stain for all the cases

Cases	Maximum strength, F_n (kN)	Deformation at the maximum capacity, d_u (mm)	Dissipated energy, G_d (kN.mm)	maximum principle plastic strain (%)
With mesh	19.8	29	334	1.237
Without mesh	9.38	19	171	1.701
A	50.06	39	1525	2.02
B	52.94	42	1602	1.152
C	19.55	28	319	1.297
D	24.52	33	566	1.011
E	16.65	27	275	1.917

In this case, PE reached the greatest value among models: 2.02%. This fact indicates that this case was the one allowing more tensile damage development in concrete. In contrast, the case with increased height of both concrete and CFRP sheet (case B) showed that tensile damage in concrete was reduced (PE 1.15%) at increasing the height of the CFRP although higher loads were predicted to be resisted. When increasing the horizontal separation between omega shapes in CFRP (case C) there was less concrete at the longitudinal edges of the case and CFRP was concentrated there reducing the possible tensile damage in concrete to PE=1.01% but reaching similar load-bearing capacity to the experimental case with mesh. The increase of the total width of the case (case D) was related to a greater ratio of concrete in the tensile area so the PE index increased up to 1.30% because tensile stresses affect a greater area. However, the increase in load-bearing capacity is directly related to the increase in the case of size in this case. Finally, removing part of the bottom plates of the CFRP sheet decreased the overlapping between CFRP and concrete, causing more tensile stresses to be assumed by the concrete without increasing its section. This combination results in a higher PE, 1.92%, but the lower load-bearing capacity among all cases with mesh. A representative contour plot of the PE index is provided in Figure 8.

5.2. Analysis of secant stiffness

As a consequence of reversal and repeated actions of monotonic loading, the stiffness of a Concrete Omega Shape slab system assembly can deteriorate. Similarly, stiffness is also reduced along with load increase when plasticization effects took place. Secant stiffness related techniques use secant stiffness at the design reaction stage and the principle of equal viscous damping to describe the non-linear behavior of structural structures [43]. Figure 9 shows how the secant or effective stiffness, Keff, is defined as the strength ratio, V*B*, to the maximum displacement possible (Figure 9). For all modeled cases the secant stiffness is taken as the slope of the straight line which connects the load at every deformation point of study with the origin. To assess this stiffness degradation, the secant stiffness is calculated at different loading stages during the simulated monotonic load increase. Relationships are represented in Figure 10. All simulated cases were compared with the experimental case with mesh in the following plots.

Simulation of the experimental cases with and without mesh showed analogous qualitative stiffness response although the embedded mesh brought a constant stiffness increase of 400kN/m respect to the case with no mesh. Cases A, B, and D showed greater stiffness than the experimental case with mesh. All of them had greater concrete area than the comparison case, being more effective, the height increase (cases A and B) than the width increase (case D), as expected. Although CFRP had a higher modulus than concrete, its area and height increase did not compensate for the reduction of the concrete area from case A to case B. This difference is reduced as tensile damage in concrete progress being no appreciated for the highest loads. Increasing the separation between omega shapes of the CFRP sheet (case C compared with the experimental case with mesh) reduced the stiffness of

the system although differences tended to decrease as load increased and the tensile damage progress. Finally, removing a significant part of the bottom CFRP (case E) was associated with the lowest stiffness all simulated test long.

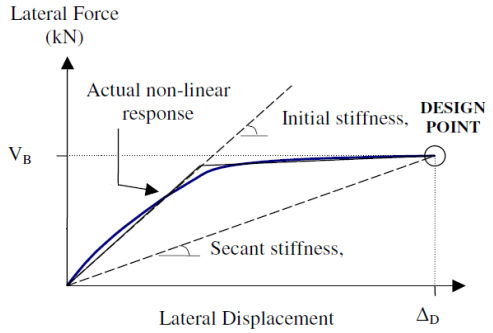

Figure 9. Usage of initial-stiffness and secant stiffness concepts related to the complete non-linear response of the structure and its equation [43]

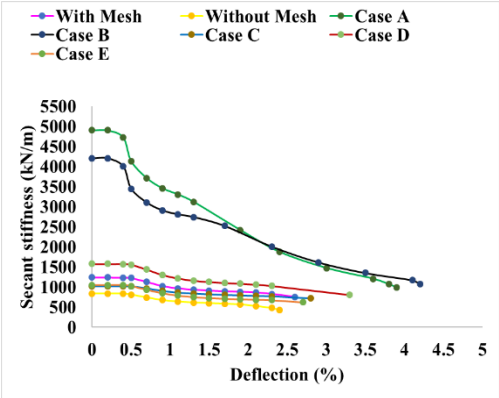

Figure 10. Secant stiffness evolution

6. Analytical methodology

Analytical post-processing of experimental data has been carried out to assess the interaction phenomenon or prove the total interaction of the tested connections. The calculations hypothesis is based on Euler-Bernoulli's assumptions of plane section and force and moment equilibrium in the calculation section. The linear-elastic response of FRP in tension and compression, the linear elastic response of mesh in tension, and the parabolic-constant response of concrete in compression were assumed. No compressive contribution of mesh neither tensile contribution of concrete was considered. Besides, total compatibility assumptions (strain continuity) were imposed in the calculation approach to assess the possibility of total interaction between concrete and FRP. First of all, a schematic representation of stress and strain distributions are included in Figure 11. For every measurement point along testing time up to failure point, the strain values at two different heights of the CFRP sheet at the center of length were used to determine the position of the neutral axis. From the position of the neutral axis, it was possible to obtain the strain distribution (linear and total compatibility hypothesis), so the corresponding stress distribution which led to the calculation of the corresponding bending moment effort obtained from the strain measurements, which was compared with the externally applied to bending moment.

Figure 12 shows a good balance between the experimental models' external moment with a calculated internal moment from proposed formulas. This evidence verifies that commonly known-by-practitioners formulations based on the Euler-Bernoulli hypothesis with total strain compatibility are applicable for the novel structural system herein analysed.

7. Conclusions

A comprehensive numerical study was carried out to investigate the performance of hybrid CFRP-concrete slabs characterized by the omega shape of the CFRP sheet. In particular, the case including flexible glass fiber mesh to connect CFRP sheet with concrete has been in-depth analyzed. After validating the model by comparison with two experimental specimens, five additional geometric definitions of hybrid CFRP-concrete slabs were simulated. Concrete Damaged Plasticity (CDP) was considered in all simulations carried out. From the pieces of evidence, the following conclusions can be drawn.

1. The proposed numerical model fitted full experimental force-displacement curves up to failure point with a slight underestimation of the maximum load-bearing capacity of less than 5%.

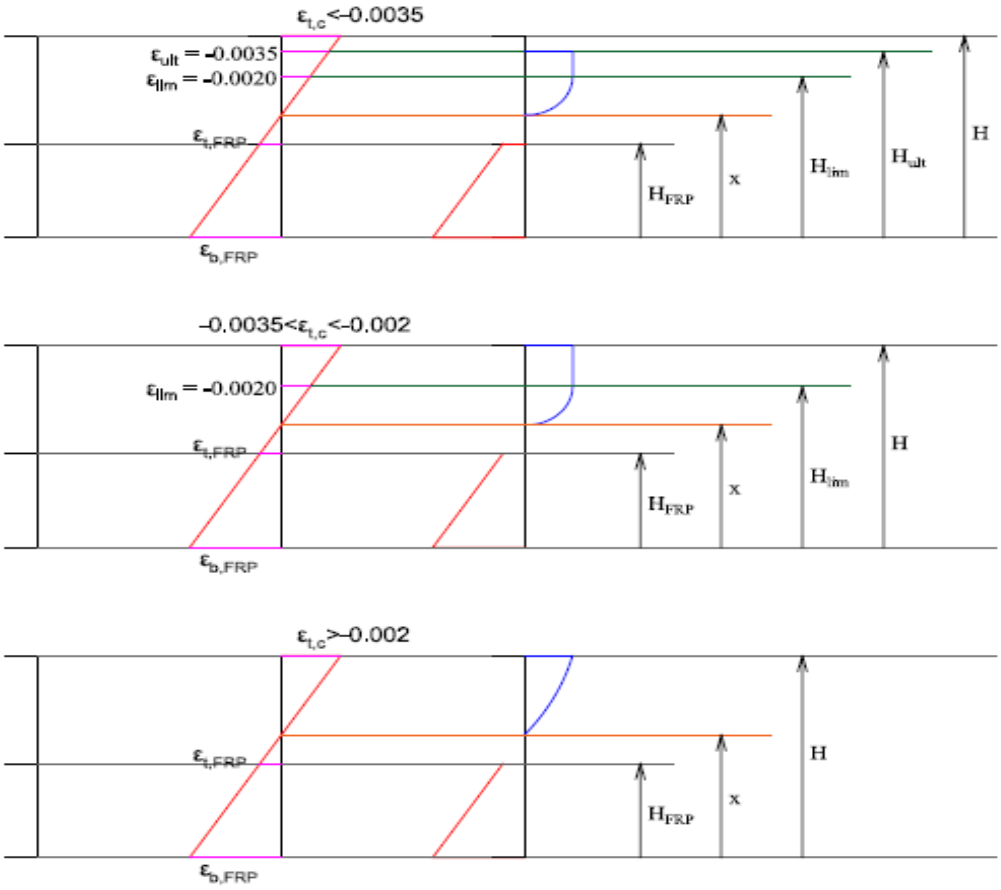

Figure 11. Strain and stress distribution for complete interaction hypothesis depending on the top concrete strain case.

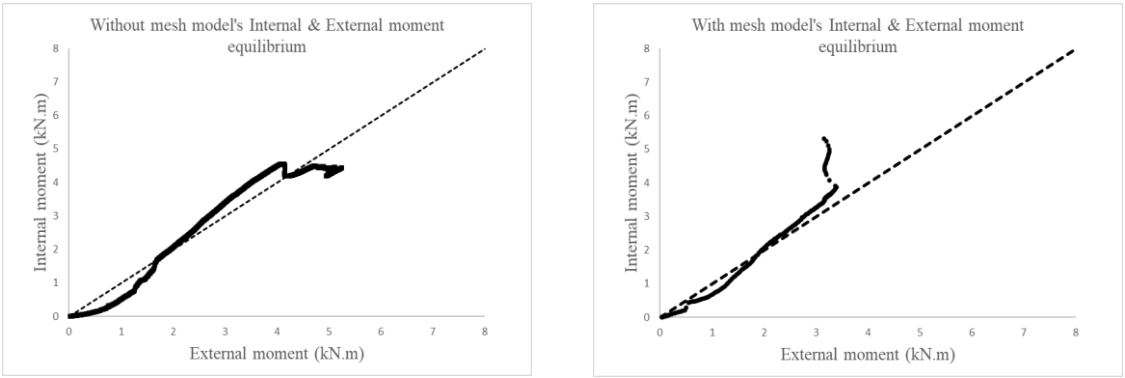

Figure 12. Experimental models' verification with proposed analytical formulas.

2. Concrete damage plasticity, dilation angle and viscosity are the most sensitive parameters to be adjusted in the numerical model.
3. Increasing the width of hybrid elements did not provide greater load-bearing capacity per unit width but a slightly stiffer response because of the higher proportion of concrete in the section. In the same reasoning line, increasing the separation between omega shape areas in the CFRP sheet was associated with no changes in the load-bearing capacity but lower initial stiffness because of the greater area of concrete in the central part of the analyzed element.
4. Increasing the height of the concrete over the CFRP omega shape sheet improved the bending capacity, reached greater concrete damage at the ultimate stage and showed the stiffest response at lower loads.
5. If the height of the CFRP omega shape sheet was simultaneously increased with the concrete height, less tensile concrete damage was predicted although final load-bearing capacity was slightly higher, and initial stiffness was lower than the case with only concrete height increase.
6. Removing part of the bottom CFRP plates was directly related to reducing the load-bearing capacity, increasing the tensile concrete damage, and lower stiffness because tensile stresses had to be supported mostly by concrete in some areas of this particular geometric definition case.
7. Analytical verifications illustrate a good balance between experimental results and calculated analytical results assuming total compatibility, so the common Euler-Bernoulli hypothesis applies to this novel CFRP sheet-concrete hybrid element typology.

References

[1] A. Mahboob, L. Gil, E. Bernat-Maso, and A. R. Eskenati, "Experimental and Numerical Study of Shear Interface Response of Hybrid Thin CFRP–Concrete Slabs," Materials, vol. 14, no. 18, p. 5184, Sep. 2021, doi: 10.3390/ma14185184.

[2] M. Abedi, O. Hassanshahi, J. A. O. Barros, A. Gomes Correia, and R. Fangueiro, "Three-dimensional braided composites as innovative smart structural reinforcements," Compos Struct, vol. 297, p. 115912, Oct. 2022, doi: 10.1016/j.compstruct.2022.115912.

[3] S. MOTAMEDPOOYA and E. ASNAASHARI, "Organizational project management maturity from the construction practitioners point of view," 2016.

[4] A. Mahboob, O. Hassanshahi, and A. S. Tabrizi, "Three-dimensional simulation of granular materials by discrete element method (DEM) by considering the fracture effect of particles," Journal of Civil Engineering Researchers, vol. 5, no. 2, pp. 14–28, 2023.

[5] A. Mahboob, O. Hassanshahi, A. Hakimi, and M. Safi, "Evaluating the Performance of Hollow Core Slabs (HCS)-Concrete and Simplifying Their Implementation," Recent Prog Mater, vol. 05, no. 02, pp. 1–15, Apr. 2023, doi: 10.21926/rpm.2302016.

[6] A. R. Eskenati, A. Mahboob, E. Bernat-Maso, and L. Gil, "Characterizing the Structural Behavior of FRP Profiles—FRCM Hybrid Superficial Elements: Experimental and Numerical Studies," Polymers (Basel), vol. 14, no. 6, p. 1076, Mar. 2022, doi: 10.3390/polym14061076.

[7] M. Veljkovic, "Behavior and resistance of composite slabs. Experiments and Finite Element Analysis," Lulea University of Technology, 1996.

[8] J. D. Ríos, H. Cifuentes, A. Martínez-De La Concha, and F. Medina-Reguera, "Numerical modelling of the shear-bond behaviour of composite slabs in four and six-point bending tests," Eng Struct, vol. 133, pp. 91–104, 2017, doi: 10.1016/j.engstruct.2016.12.025.

[9] S. Chen and X. Shi, "Shear bond mechanism of composite slabs - A universal FE approach," J Constr Steel Res, vol. 67, no. 10, pp. 1475–1484, 2011, doi: 10.1016/j.jcsr.2011.03.021.

[10] A. Mahboob, A. R. Eskenati, and S. Moradalizadeh, "Numerical Investigation and Cost Analysis of FRP-Concrete Unidirectional Hybrid Slabs," International Journal of Applied Mechanics and Engineering, vol. 26, no. 4, pp. 156–166, Dec. 2021, doi: 10.2478/ijame-2021-0056.

[11] S. Abbasi, A. Mahboob, H. Bakhtiari Zamani, M. R. Bilesan, E. Repo, and A. Hakimi, "The Tribological Behavior of Nanocrystalline TiO2 Coating Produced by Plasma Electrolytic Oxidation," J Nanomater, vol. 2022, pp. 1–13, Jan. 2022, doi: 10.1155/2022/5675038.

[12] M. Abedi et al., "A self-sensing and self-heating planar braided composite for smart civil infrastructures reinforcement," Constr Build Mater, vol. 387, p. 131617, Jul. 2023, doi: 10.1016/j.conbuildmat.2023.131617.

[13] A. Salles, M. Salati, and L. Bragança, "Analyzing the Feasibility of Integrating Urban Sustainability Assessment Indicators with City Information Modelling (CIM)," Applied System Innovation, vol. 6, no. 2, p. 45, Mar. 2023, doi: 10.3390/asi6020045.

[14] M. Salati, L. Bragança, and R. Mateus, "Sustainability Assessment on an Urban Scale: Context, Challenges, and

Most Relevant Indicators," Applied System Innovation, vol. 5, no. 2, p. 41, Apr. 2022, doi: 10.3390/asi5020041.
[15] M. Abedi et al., "A sustainable cementitious composite reinforced with natural fibers: An experimental and numerical study," Constr Build Mater, vol. 378, p. 131093, May 2023, doi: 10.1016/j.conbuildmat.2023.131093.
[16] C. L. Oh, K. K. Choong, T. Nishimura, J.-Y. Kim, and O. Hassanshahi, "Shape change analysis of tensegrity models," Latin American Journal of Solids and Structures, vol. 16, no. 7, 2019, doi: 10.1590/1679-78255407.
[17] A. R. Eskenati, A. Mahboob, E. Bernat-Maso, and L. Gil, "Experimental and Numerical Study of Adhesively and Bolted Connections of Pultruded GFRP I-Shape Profiles," Polymers (Basel), vol. 14, no. 5, p. 894, Feb. 2022, doi: 10.3390/polym14050894.
[18] A. Yousefi, N. M. Bunnori, M. Khavarian, O. Hassanshahi, and T. A. Majid, "Experimental investigation on effect of multi-walled carbon nanotubes concentration on flexural properties and microstructure of cement mortar composite," 2017, p. 020032. doi: 10.1063/1.5005663.
[19] M. Golabchi and E. Asnaashari, "Identification of Iran's road construction project risks in order to implement sustainable development (Pavement Technologies and Construction Activities)".
[20] W. Y. Peen, C. K. Keong, and O. Hassanshahi, "Behaviour of hollow circular section with multiple perforations under compression, flexure and torsion," Latin American Journal of Solids and Structures, vol. 16, no. 2, 2019, doi: 10.1590/1679-78255387.
[21] A. Mahboob, L. Gil, E. Bernat-Maso, and A. R. Eskenati, "Flexible Fiber Fabric for FRP–Concrete Connection of Thin Hybrid Slabs," Polymers (Basel), vol. 13, no. 17, p. 2862, Aug. 2021, doi: 10.3390/polym13172862.
[22] A. R. Eskenati, A. Mahboob, A. Alirezaie, R. Askari, and S. M. S. Kolbadi, "INVESTIGATING THE EFFECT OF LONGITUDINAL GALLERY ON DYNAMICAL RESPONSE OF GRAVITY CONCRETE DAMS USING FEM," Journal of Southwest Jiaotong University, vol. 56, no. 4, pp. 804–811, Aug. 2021, doi: 10.35741/issn.0258-2724.56.4.69.
[23] O. Hassanshahi, T. A. Majid, T. L. Lau, A. Yousefi, and R. M. K. Tahara, "Seismic performance of the typical RC beam–column joint subjected to repeated earthquakes," 2017, p. 120014. doi: 10.1063/1.5005755.
[24] CEB-FIP MODEL CODE 1990. 1993. doi: 10.1680/ceb-fipmc1990.35430.
[25] ASTMD3531, "Standard Test Method for Resin Flow of Carbon Fiber-Epoxy Prepreg," Annual book of ASTM standards, 2014.
[26] ASTM Committee D30.05, "ASTM D7565-10 Standard Test Method for Determining Tensile Properties of Fiber Reinforced Polymer Matrix Composites Used for Strengthening of Civil Structures," in Annual Book of ASTM Standards Volume 15.03, 2010. doi: 10.1520/D7565_D7565M-10.
[27] Hibbitt Karlsson & Sorensen inc., ABAQUS / Explicit User ' s Manual. Inso Corporation, 2000.
[28] J. Lubliner, J. Oliver, S. Oller, and E. Oñate, "A plastic-damage model for concrete," Int J Solids Struct, vol. 25, no. 3, pp. 299–326, Jan. 1989, doi: 10.1016/0020-7683(89)90050-4.
[29] J. Lee and G. L. Fenves, "Plastic-Damage Model for Cyclic Loading of Concrete Structures," J Eng Mech, vol. 124, no. 8, pp. 892–900, Aug. 1998, doi: 10.1061/(ASCE)0733-9399(1998)124:8(892).
[30] J. Lee and G. L. Fenves, "Plastic-Damage Model for Cyclic Loading of Concrete Structures," J Eng Mech, vol. 124, no. 8, pp. 892–900, Aug. 1998, doi: 10.1061/(ASCE)0733-9399(1998)124:8(892).
[31] Y. Sümer, M. A.-C. J. of Structural, and U. 2015, "Defining parameters for concrete damage plasticity model," Challenge Journal of Structural Mechanics, 2015, doi: 10.20528/cjsmec.2015.07.023.
[32] G. Zhao and A. Li, "Numerical study of a bonded steel and concrete composite beam," Comput Struct, vol. 86, no. 19–20, pp. 1830–1838, Oct. 2008, doi: 10.1016/j.compstruc.2008.04.002.
[33] M. H. Seleem, I. A. Sharaky, and H. E. M. Sallam, "Flexural behavior of steel beams strengthened by carbon fiber reinforced polymer plates - Three dimensional finite element simulation," Mater Des, vol. 31, no. 3, pp. 1317–1324, Mar. 2010, doi: 10.1016/j.matdes.2009.09.010.
[34] I. Vilanova, L. Torres, M. Baena, and M. Llorens, "Numerical simulation of bond-slip interface and tension stiffening in GFRP RC tensile elements," Compos Struct, vol. 153, pp. 504–513, 2016, doi: 10.1016/j.compstruct.2016.06.048.
[35] D. C. Kent and R. Park, "FLEXURAL MEMBERS WITH CONFINED CONCRETE," Journal of the Structural Division, Jul. 1971.
[36] R. Massarelli, J. E. Franquet, K. Shrestha, R. Tremblay, and C. A. Rogers, "Seismic testing and retrofit of steel deck roof diaphragms for building structures," Thin-Walled Structures, vol. 61, pp. 239–247, 2012, doi: 10.1016/j.tws.2012.05.013.
[37] X. Wang, C. Su, W. Deng, and Z. Wu, "Bond behavior between corrugated BFRP shell and concrete under monotonic and cyclic loads," Constr Build Mater, vol. 210, pp. 596–606, 2019, doi: 10.1016/j.conbuildmat.2019.03.072.
[38] Y. Ou, J. M. Gattas, D. Fernando, and J. L. Torero, "Experimental investigation of a timber-concrete floor panel system with a hybrid glass fibre reinforced polymer-timber corrugated core," Eng Struct, vol. 203, no. November 2019, 2020, doi: 10.1016/j.engstruct.2019.109832.
[39] B. W. Schafer, Z. Li, and C. D. Moen, "Computational modeling of cold-formed steel," Thin-Walled Structures, vol. 48, no. 10–11, pp. 752–762, 2010, doi: 10.1016/j.tws.2010.04.008.
[40] Hibbitt Karlsson & Sorensen inc., ABAQUS/Standard: User's Manual. Inso Corporation, 1998.
[41] H. Behnam, J. S. Kuang, and B. Samali, "Parametric finite element analysis of RC wide beam-column connections," Comput Struct, vol. 205, pp. 28–44, 2018, doi: 10.1016/j.compstruc.2018.04.004.
[42] Y. Liu, M. Zhang, X. Yin, Z. Huang, and L. Wang, "Debonding Performance of CFRP-Strengthened Nanomaterial Concrete Beam Using Wavelet Packet

Analysis," J Sens, vol. 2020, 2020, doi: 10.1155/2020/7526703.
[43] G. H. Powell, "Displacement-Based Seismic Design of Structures," Earthquake Spectra, 2008, doi: 10.1193/1.2932170.